An isogeometric indirect boundary element method for Helmholtz problems

L. Coox [1], **O. Atak** [1], **D. Vandepitte** [1], **W. Desmet** [1]
[1] KU Leuven, Department of Mechanical Engineering,
Celestijnenlaan 300B, B-3001, Heverlee, Belgium
e-mail: **laurens.coox@kuleuven.be**

Abstract

Isogeometric Analysis (IGA) is a recently introduced concept that tries to bridge the gap between Computer Aided Engineering (CAE) and Computer Aided Design (CAD). It does so by generalising the Finite Element Method (FEM) to describe the problem geometry with functions that are typically used in CAD environments (such as NURBS) and then using the same type of functions to represent the field variables — often invoking the isoparametric paradigm. This concept allows to bypass the labor-intensive step of converting a CAD geometry to an analysis-suitable geometry description, which is usually a huge bottleneck in the conventional FEM. Moreover, IGA has been shown to exhibit several advantageous approximation properties over the FEM for analysing problems in various fields of research. This paper studies whether these interesting results can be extended to Helmholtz problems using a boundary element formulation. More specifically, this work integrates the isogeometric idea in an indirect variational Boundary Element Method (BEM) for steady-state acoustic problems involving surfaces with open boundaries. The numerical results show that the proposed method compares favorably to a traditional Lagrangian BEM, exhibiting a significantly higher accuracy per degree of freedom.

1 Introduction

The vibro-acoustic performance of a product has long been treated at the end of the design process – when it was usually too late to make significant product modifications if performance turned out insufficient. However, due to ever more stringent regulations on noise emission and exposure to vibration levels, and to the use of new (lighter) types of construction materials, the vibro-acoustic behaviour has become an important factor in product design in recent years. The availability of ever more performant computer systems has made Computer Aided Engineering (CAE) techniques indispensable to design engineers, allowing them to predict product performance with satisfying accuracy, even early on during the design stage. Current state-of-the-use CAE tools (in a.o. acoustic problems) are the Finite Element Method (FEM) [1] and the Boundary Element Method (BEM) [2].

Although CAE has led to significantly shorter design cycles, there is still a lot of room for improvement. Despite the fact that the FEM takes the product geometry as a starting point, the current Computer Aided Design (CAD) techniques were developed after the FEM had been established as an analysis method. Because CAD and the FEM have grown up independently from each other, geometric representations in CAD and the FEM are very different. An incompatibility remains between them, which requires a tedious and time-consuming conversion step between the two, i.e. meshing of the geometry, in order to obtain an analysis-suitable geometry. Especially for problems of industrial complexity, this meshing process can form a real bottleneck, taking up to $80\,\%$ of the total analysis time [3]. Moreover, if mesh refinement is required, communication

with the CAD model is necessary, which is often difficult and sometimes not even possible. In designing today's ever more complex products, where optimisation iterations are often required, this gap between CAD and CAE can drastically slow down product development cycles.

Isogeometric analysis (IGA) [3,4] aims at bridging this gap between design and analysis by introducing CAD descriptions into a CAE environment. The conventional element-based discretisation and the associated (usually low-order polynomial) shape function expansions in the FEM are replaced by CAD-based mappings and associated functions, typically spline-based functions. The underlying idea, however, of minimising the error of approximation typically by applying the Galerkin method of weighted residuals, remains the same. Also the assembly of element arrays into global arrays in IGA can be done in the same way as in the FEM. In that sense, IGA can be considered as a generalisation of the traditional FEM. The first implementations of IGA [3] were based on Non-Uniform Rational B-Splines (NURBS), one of the most widely used computational geometry representations in engineering designs. Mathematical studies of IGA formulations were presented in [5, 6]. NURBS have been shown to possess advantageous properties for analysis purposes, and IGA has already attained excellent results in various fields of study, such as structural mechanics [7–9], turbulent flow problems [10, 11] and fluid-structure interaction [5, 12]. Although still a young technique, IGA is rapidly becoming a mainstream analysis methodology, and the isogeometric concept has also been implemented in boundary element formulations [14, 15]. A direct boundary element method for acoustic problems using an isogeometric approach with T-splines is presented in [13]. This direct boundary integral formulation, however, is limited to closed boundary surfaces and either interior or exterior acoustic problems, whereas various industrial problems require the modelling of open boundary problems. An indirect variational formulation of the BEM [2] (also referred to as symmetric Galerkin BEM), on the other hand, is capable of modelling such problems.

As such, this paper introduces a novel isogeometric indirect variational BEM for steady-state acoustic problems, and reports on its performance as compared to a traditional Lagrangian BEM. One of the driving factors for the use of a boundary element formulation is the fact that CAD descriptions are typically boundary descriptions. Even for volumetric objects, CAD tools only describe the envelope surface, which is not always sufficient for analysis purposes. This makes a boundary element formulation inherently well-suited for implementing the isogeometric concept.

The rest of this paper is structured as follows: The next section describes a general acoustic problem as studied in this work. After that, the isogeometric methodology is described in more detail, followed by the proposed boundary element method that is implemented in this study. The subsequent section presents a numerical verification case, to finish with some concluding remarks.

2 Problem definition

Consider a general (unbounded) steady-state acoustic problem as depicted in Figure 1. The acoustic domain V is filled with an acoustic fluid characterised by its speed of sound c and its fluid mass density ρ_0. The steady-state dynamic behaviour in this acoustic domain is described by the acoustic pressure field $p_a(\boldsymbol{r})$, which is governed by the inhomogeneous Helmholtz equation [16]:

$$\nabla^2 p_a(\boldsymbol{r}) + k^2 p_a(\boldsymbol{r}) = -\mathrm{j}\rho_0\omega q\delta(\boldsymbol{r}, \boldsymbol{r_q}), \qquad \boldsymbol{r} \in V, \tag{1}$$

where $\boldsymbol{r}$ is the position vector, k the acoustic wavenumber, ω the angular frequency, q the strength of an acoustic volume velocity source at position $\boldsymbol{r_q}$, and $\delta(\bullet, \star)$ the Dirac-delta function. The speed of sound $c = \frac{\omega}{k}$ relates the angular frequency ω to the wavenumber k. The term $\nabla^2\bullet = \frac{\partial^2\bullet}{\partial x^2} + \frac{\partial^2\bullet}{\partial y^2} + \frac{\partial^2\bullet}{\partial z^2}$ is the Laplacian operator and j denotes the imaginary unit ($\mathrm{j}^2 = -1$).

In order to have a unique solution, the Helmholtz equation (1) requires one imposed boundary condition at each point on the problem boundary $\Omega = \partial V$. In the case of an unbounded fluid domain, as in Figure 1, the problem boundary consists of two parts: (i) the finite part of the boundary, Ω_f, and (ii) the boundary

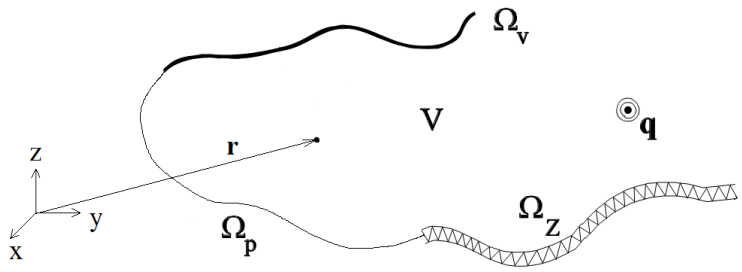

Figure 1: Description of an (unbounded) acoustic problem.

at infinity, Ω_∞. Evidently, for a bounded fluid domain, only Ω_f has to be considered. The finite part Ω_f of the problem boundary can be divided into three non-overlapping parts, assuming three types of common acoustic boundary conditions: $\Omega_f = \Omega_p \cup \Omega_v \cup \Omega_Z$. The boundary condition on Ω_f can then be written as follows:

$$p_a(\boldsymbol{r}) = \bar{p}_a \qquad \boldsymbol{r} \in \Omega_p, \tag{2}$$

$$\frac{\mathrm{j}}{\rho_0 \omega} \frac{\partial p_a(\boldsymbol{r})}{\partial \boldsymbol{n}} = \bar{v}_n \qquad \boldsymbol{r} \in \Omega_v, \tag{3}$$

$$\frac{\mathrm{j}}{\rho_0 \omega} \frac{\partial p_a(\boldsymbol{r})}{\partial \boldsymbol{n}} = \frac{p_a(\boldsymbol{r})}{\bar{Z}_n} \qquad \boldsymbol{r} \in \Omega_Z. \tag{4}$$

The quantities $\bar{p}_a$, $\bar{v}_n$ and $\bar{Z}_n$ are the imposed pressure, imposed normal velocity and imposed normal impedance, respectively. $\boldsymbol{n}$ is the normal vector on the boundary. At the boundary at infinity Ω_∞, non-reflecting boundary conditions are imposed. This ensures that no energy is reflected back into the problem domain and that the resulting acoustic waves can propagate freely towards infinity. This is known as the Sommerfeld radiation condition:

$$\lim_{\boldsymbol{r} \to \infty} \left(\frac{\partial p_a}{\partial \boldsymbol{n}} + \mathrm{j} k p_a \right) = 0 \tag{5}$$

The Helmholtz equation (1) together with the boundary conditions (2) – (5) fully define the acoustic pressure field $p_a(\boldsymbol{r})$ in the entire problem domain.

3 Basic NURBS terminology for isogeometric analysis

The presented indirect boundary element method uses NURBS for both the geometry description and the representation of the field variables. This section introduces the basics of NURBS curves and surfaces with their corresponding functions in the context of IGA. First the construction of NURBS is discussed here, then their main features that are of importance in IGA. The interested reader can find a more detailed explanation in [4, 17].

3.1 From B-splines to NURBS

NURBS are built from B-splines. A B-spline curve of polynomial order p is defined by a knot vector and a set of control points. A knot vector Ξ is a non-decreasing set of coordinates in the parameter space, $\Xi = [\xi_1, \xi_2, \ldots, \xi_{n+p+1}]$, where $\xi_i \in \mathbb{R}$ is the i^{th} knot, with i the knot index ($i = 1, 2, \ldots, n+p+1$) and n the number of basis functions making up the B-spline. Open knot vectors, where the first and the last knot each appear $p+1$ times, are standard in CAD. Starting from a knot vector, B-spline basis functions $N_i^p(\xi)$

($i = 1, \ldots, n$) are defined recursively using the Cox – de Boor recursion formula:

$$\begin{aligned} p = 0: \quad & N_i^0(\xi) = \begin{cases} 1 & \xi_i \leq \xi < \xi_{i+1} \\ 0 & \text{otherwise} \end{cases}, \\ p > 0: \quad & N_i^p(\xi) = \frac{\xi - \xi_i}{\xi_{i+p} - \xi_i} N_i^{p-1}(\xi) + \frac{\xi_{i+p+1} - \xi}{\xi_{i+p+1} - \xi_{i+1}} N_{i+1}^{p-1}(\xi). \end{aligned} \tag{6}$$

Note that these functions are piecewise polynomials. B-spline curves in $\mathbb{R}^{\mathrm{d}}$ are simply a linear combination of these n basis functions, where the control points $\mathbf{B}_i^{\mathbf{w}} \in \mathbb{R}^{\mathrm{d}}$ ($i = 1, \ldots, n$) represent the vector-valued weighting coefficients. A B-spline curve $C^w(\xi)$ is then given by

$$C^w(\xi) = \sum_{i=1}^{n} N_i^p(\xi) \mathbf{B}_i^{\mathbf{w}}. \tag{7}$$

A B-spline surface $S^w(\xi, \eta)$ is a tensor product surface of two univariate B-splines. Given a net of control points $\mathbf{B}_{i,j}^{\mathbf{w}}$ ($i = 1, \ldots, n$, $j = 1, \ldots, m$), polynomial orders p and q, and a pair of knot vectors $\Xi = [\xi_1, \xi_2, \ldots, \xi_{n+p+1}]$ and $H = [\eta_1, \eta_2, \ldots, \eta_{m+q+1}]$, it is defined as

$$S^w(\xi, \eta) = \sum_{i=1}^{n} \sum_{j=1}^{m} N_i^p(\xi) M_j^q(\eta) \mathbf{B}_{i,j}^{\mathbf{w}}, \tag{8}$$

where $N_i^p(\xi)$ and $M_j^q(\eta)$ represent univariate B-spline basis functions of order p and q, associated with knot vectors Ξ and H, respectively. Analogously, a B-spline volume is defined as a tensor product of three univariate B-splines.

A projective transformation of a B-spline entity in $\mathbb{R}^{\mathrm{d+1}}$ renders NURBS entities in $\mathbb{R}^{\mathrm{d}}$. The details are omitted here, but the NURBS basis can be derived from a B-spline basis by defining a weight w_i for every B-spline basis function, which in turn define a weighting function. The NURBS basis functions $R_i^p(\xi)$ of polynomial order p are then given by

$$R_i^p(\xi) = \frac{N_i^p(\xi) w_i}{W(\xi)} = \frac{N_i^p(\xi) w_i}{\sum_{i=1}^{n} N_i^p(\xi) w_i}, \tag{9}$$

with $W(\xi)$ the weighting function. $R_i^p(\xi)$ are piecewise rational functions, since $N_i^p(\xi)$ and $W(\xi)$ are both piecewise polynomial functions. The NURBS curve $C(\xi)$ associated with these basis functions and with control points $\mathbf{B}_i \in \mathbb{R}^{\mathrm{d}}$ is then, completely analogous to a B-spline curve, defined as

$$C(\xi) = \sum_{i=1}^{n} R_i^p(\xi) \mathbf{B}_i. \tag{10}$$

It is worth noting that if all the weights are equal, then $R_{i,p}(\xi) = N_{i,p}(\xi)$. The basis functions are again polynomials and the NURBS degenerates into a B-spline. B-splines are therefore a special case of NURBS.

Analogously as for B-splines, a NURBS surface or volume can be defined as the tensor product of univariate NURBS. The basis functions for a NURBS surface $S(\xi, \eta)$ then become

$$R_{i,j}^{p,q}(\xi, \eta) = \frac{N_i^p(\xi) M_j^q(\eta) w_{i,j}}{\sum_{\hat{i}=1}^{n} \sum_{\hat{j}=1}^{m} N_{\hat{i}}^p(\xi) M_{\hat{j}}^q(\eta) w_{\hat{i},\hat{j}}}, \tag{11}$$

yielding

$$S(\xi, \eta) = \sum_{i=1}^{n} \sum_{j=1}^{m} R_{i,j}^{p,q}(\xi, \eta) \mathbf{B}_{i,j}. \tag{12}$$

Applying the isoparametric paradigm, these same NURBS basis functions can also be used in the shape function expansion for representing the field variables.

3.2 Main features of NURBS

A general NURBS surface can consist of a combination of several NURBS surfaces, or patches, each of which is defined as in equation (12). Each patch is a concatenation of knot spans. These are delimited by (non-identical) knots and represent the elements in the mesh, where the basis functions are smooth (i.e. C^∞-continuous). Across a knot ξ_i, the basis functions have a C^{p-m} continuity, with m the multiplicity of knot ξ_i. NURBS bases are therefore quite flexible regarding inter-element continuity, and virtually arbitrarily high inter-element continuities can be obtained.

One of the main differences with traditional FEM and BEM shape functions is that NURBS are in general not interpolatory. The degrees of freedom are therefore called control variables instead of nodal variables. A NURBS basis function can also span several elements, whereas traditional FEM and BEM shape functions are only locally defined within one element.

Another important difference is that unlike standard polynomials, the NURBS parameter space is local to patches rather than elements. Whereas in the FEM or BEM each element is mapped from one parent element onto a single element in the physical space according to its own geometric mapping, a NURBS mapping applies to the entire patch: each element in the physical space is mapped from its corresponding element in parameter space.

An additional advantage of NURBS functions is that they allow for an extra refinement technique. There are the analogues of classical h-refinement (knot insertion) and p-refinement (order elevation) of the traditional FEM, but there is also a new possibility reffered to as k-refinement. This technique first increases the polynomial order and then inserts knots. This also increases smoothness of the basis and has no analogue in traditional FEM or BEM approaches. The concept of k-refinement seems to exhibit better efficiency and robustness over traditional p-refinement [3].

4 An isogeometric indirect boundary element method

This section presents the proposed isogeometric boundary element method. The first part discusses the BEM for solving time-harmonic acoustic problems in general, in particular the indirect variational BEM and specifically for unbounded problems[1]. After that, the implementation of the isogeometric indirect variational BEM is discussed.

4.1 The indirect variational boundary element method in acoustics

The BEM [2], like the FEM, is an element-based prediction technique, but unlike the FEM it uses a boundary integral formulation of the problem under study. This formulation relates the field variables in the continuum domain to the distribution of associated boundary variables on the boundary surface of the domain. Therefore the BEM requires only the boundary to be discretised into elements instead of the entire acoustic domain. While the resulting system matrices are fully populated, complex and frequency dependent, this feature can significantly decrease the number of Degrees Of Freedom (DOFs). Moreover, in representing the field variables, the BEM uses Green's kernel functions, which inherently satisfy the Sommerfeld radiation condition (5). This makes the BEM especially well suited for modelling unbounded acoustic problems.

The proposed method uses an indirect variational formulation of the boundary integral. This allows the modelling of problems with open boundary surfaces. An exterior acoustic problem with an open boundary surface can be regarded as a special case of an exterior problem with a closed boundary by viewing both surface sides as two separate parts of a closed boundary surface. Figure 2 illustrates this. The indirect

[1] By regarding the total inhomogeneous pressure field as a superposition of a homogeneous pressure field and an inhomogeneous free-field pressure, a numerical solution procedure is required only for the homogeneous problem (after reformulating the boundary conditions for the total pressure in terms of the homogeneous pressure field). The remaining part of this section therefore assumes a homogeneous acoustic problem, without loss of generality.

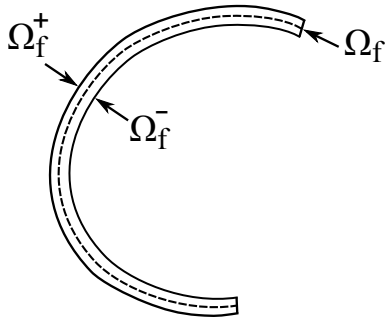

Figure 2: Boundary description for an open boundary surface in an indirect boundary integral formulation.

boundary integral formulation uses the difference in pressure and in normal pressure gradient between the two sides as primary variables. These variables are called the double layer potential $\mu(\boldsymbol{r}_f)$ and the single layer potential $\sigma(\boldsymbol{r}_f)$, respectively: [2]

$$\mu(\boldsymbol{r}_f) = p_a(\boldsymbol{r}_f^+) - p_a(\boldsymbol{r}_f^-) \qquad \boldsymbol{r}_f \in \Omega_f, \tag{13}$$

$$\sigma(\boldsymbol{r}_f) = \frac{\partial p_a(\boldsymbol{r}_f^+)}{\partial \boldsymbol{n}} - \frac{\partial p_a(\boldsymbol{r}_f^-)}{\partial \boldsymbol{n}} \qquad \boldsymbol{r}_f \in \Omega_f, \tag{14}$$

with $\boldsymbol{r}_f$ the position vector on the boundary surface. Assuming a thin boundary surface, boundary conditions (2) – (4) can be reformulated in terms of the single and the double layer potential as:

$$\mu(\boldsymbol{r_f}) = 0 \qquad \boldsymbol{r_f} \in \Omega_p, \tag{15}$$

$$\sigma(\boldsymbol{r_f}) = 0 \qquad \boldsymbol{r_f} \in \Omega_v, \tag{16}$$

$$\sigma(\boldsymbol{r_f}) = -\mathrm{j}k\bar{\beta}\mu(\boldsymbol{r_f}) \qquad \boldsymbol{r_f} \in \Omega_Z, \tag{17}$$

where $\bar{\beta} = \rho_0 c/\bar{Z}_n$. The indirect boundary integral formulation, relating the pressure in any point of the acoustic domain to the distributions of the single and the double layer potential on the boundary surface, can then be written as:

$$\begin{aligned} p_a(\boldsymbol{r}) = &- \int_{\Omega_p} \sigma(\boldsymbol{r_f}) G(\boldsymbol{r}, \boldsymbol{r}_f) \mathrm{d}\Omega_f(\boldsymbol{r}_f) + \int_{\Omega_v} \mu(\boldsymbol{r_f}) \frac{\partial G(\boldsymbol{r}, \boldsymbol{r}_f)}{\partial \boldsymbol{n}} \mathrm{d}\Omega_f(\boldsymbol{r}_f) \\ &+ \int_{\Omega_Z} \mu(\boldsymbol{r_f}) \left(\frac{\partial G(\boldsymbol{r}, \boldsymbol{r}_f)}{\partial \boldsymbol{n}} + \mathrm{j}k\bar{\beta}(\boldsymbol{r}_f) G(\boldsymbol{r}, \boldsymbol{r}_f) \right) \mathrm{d}\Omega_f(\boldsymbol{r}_f). \end{aligned} \tag{18}$$

This formulation makes use of the Green's kernel function $G(\boldsymbol{r}, \boldsymbol{r}_f)$, which represents the free-field pressure in any point $\boldsymbol{r}$ due to an acoustic point source in $\boldsymbol{r}_f$. It is defined as follows for three-dimensional domains:

$$G(\boldsymbol{r}, \boldsymbol{r}_f) = \frac{\mathrm{e}^{-\mathrm{j}k|\boldsymbol{r}-\boldsymbol{r}_f|}}{4\pi\,|\boldsymbol{r} - \boldsymbol{r}_f|}. \tag{19}$$

To determine the distributions of the single and the double layer potential on the boundary surface, the boundary conditions (2) – (4) have to be enforced using equation (18), leading to three integral equations that have to be solved for $\mu(\boldsymbol{r}_f)$ and $\sigma(\boldsymbol{r}_f)$. The details are omitted here — the interested reader is referred to [2] — but a weighted residual formulation of those integral equations is:

$$\forall\,(\delta\sigma, \delta\mu) : \int_{\Omega_p} R_p(\sigma, \mu)\delta\sigma \mathrm{d}\Omega_f + \int_{\Omega_v} R_v(\sigma, \mu)\delta\mu \mathrm{d}\Omega_f + \int_{\Omega_Z} R_Z(\sigma, \mu)\delta\mu \mathrm{d}\Omega_f = 0, \tag{20}$$

where $R_p(\sigma, \mu)$, $R_v(\sigma, \mu)$ and $R_Z(\sigma, \mu)$ are the boundary residuals for the Dirichlet, Neumann and Robin boundaries, respectively. The terms $\delta\sigma$ and $\delta\mu$ are test functions. Solving this equation for $\sigma(\boldsymbol{r}_f)$ on $\Omega_\sigma = \Omega_p$ and for $\mu(\boldsymbol{r}_f)$ on $\Omega_\mu = \Omega_v \cup \Omega_Z$ yields the distributions of the single and the double layer potential on the boundary surface.

4.2 Integrating the isogeometric concept in the boundary element formulation

To numerically solve equation (20), the boundary surfaces Ω_σ and Ω_μ are discretised into boundary elements. The potentials $\sigma(\boldsymbol{r}_f)$ and $\mu(\boldsymbol{r}_f)$ are then approximated by shape function expansions $\hat{\sigma}(\boldsymbol{r}_f)$ and $\hat{\mu}(\boldsymbol{r}_f)$:

$$\sigma(\boldsymbol{r}_f) \approx \hat{\sigma}(\boldsymbol{r}_f) = \sum_{i=1}^{n_{\sigma d}} N_{\sigma,i}(\boldsymbol{r}_f) \cdot d_{\sigma,i} \qquad \boldsymbol{r}_f \in \Omega_\sigma, \tag{21}$$

$$\mu(\boldsymbol{r}_f) \approx \hat{\mu}(\boldsymbol{r}_f) = \sum_{i=1}^{n_{\mu d}} N_{\mu,i}(\boldsymbol{r}_f) \cdot d_{\mu,i} \qquad \boldsymbol{r}_f \in \Omega_\mu, \tag{22}$$

where $n_{\bullet d}$ is the number of (prescribed) shape functions in the expansion. Using an isoparametric representation, these shape functions are the same as the ones used for the problem geometry mapping. Following a Galerkin approach, the same shape functions are then used for the test functions. In the traditional Lagrangian BEM, the shape functions $N_{\bullet,i}$ (with associated contribution factors $d_{\bullet,i}$) are Lagrangian polynomials that are only locally defined within one boundary element: They have unit value at one node and zero at all the other ones, making $d_{\bullet,i}$ nodal DOFs. In contrast, the proposed method uses NURBS shape functions as in equation (9), which, although also highly locally supported, typically span several elements. A consequence of this wider support is that the shape functions are in general not interpolatory, and the contribution factors $d_{\bullet,i}$ (called the control variables in IGA terminology) are therefore not nodal DOFs anymore.

By introducing the shape function expansions (21) and (22) into the weighted residual formulation (20) and by using a Galerkin approach, a global system of equations can be assembled. Solving this for $d_{\bullet,i}$ yields the discretised single layer potential $\hat{\sigma}(\boldsymbol{r}_f)$ and double layer potential $\hat{\mu}(\boldsymbol{r}_f)$. Post-processing this using equation (18) allows for calculating the pressure at any position inside the acoustic domain.

The non-interpolatory properties of the NURBS basis also have consequences for applying essential boundary conditions. Consider a Dirichlet boundary condition $\mu(\boldsymbol{r}_f) = g(\boldsymbol{r}_f)$ on $\boldsymbol{r}_f \in \Omega_\mu$. The function g does not necessarily lie within the function space $\mathcal{S}^h$ spanned by the NURBS basis, i.e. there might not exist a function $g^h \in \mathcal{S}^h$ such that $g^h|_{\Omega_\mu} = g$. The Dirichlet boundary condition will then be only approximatively satisfied: $g^h|_{\Omega_\mu} \approx g$. The traditional FEM and BEM satisfy such boundary conditions pointwise by interpolating g at the boundary nodes. In IGA, however, this can lead to a smeared g^h. Alternatively, a weakly imposed Dirichlet condition could be used [4]. Luckily, homogeneous Dirichlet conditions ($g = 0$) do not pose a problem, since they can easily be built into the solution space by applying them to the control variables, i.e. setting the contribution factors of all functions N_{μ,i,Ω_μ} that are non-zero on Ω_μ to zero: $d_{\mu,i,\Omega_\mu} = 0$. The partition of unity of the basis then ensures that $\mu(\boldsymbol{r}_f) = 0$ on $\boldsymbol{r}_f \in \Omega_\mu$ — the same reasoning holds for non-homogeneous but constant Dirichlet conditions. This is important in the proposed technique for applying a zero jump of pressure condition at free edges of an open boundary domain, i.e. $\mu(\boldsymbol{r}_f|_{\Gamma(\Omega_f)}) = 0$, with $\Gamma(\Omega_f)$ the free boundary edges. As such, these boundary conditions are exactly satisfied.

5 Numerical verification

In order to verify the accuracy of the proposed isogeometric indirect variational BEM and to evaluate its performance compared to the conventional Lagrangian BEM, simulations are carried out for a verification case shown in Figure 3. It is an exterior acoustic problem with an open boundary surface, more specifically a zero thickness panel of dimensions of $1\,\mathrm{m} \times 1\,\mathrm{m}$ which is curved in one direction with a curvature radius of $0.5\,\mathrm{m}$. It acts as a rigid boundary ($\bar{v}_n = 0$) and it is surrounded by air ($\rho_0 = 1.225\,\mathrm{kg/m^3}$, $c = 340\,\mathrm{m/s}$). The acoustic domain is excited by a unit point source located at $\boldsymbol{r}_q$.

The resulting acoustic pressure field is studied in a frequency range from 50 to $500\,\mathrm{Hz}$. Three different simulations are performed with the proposed method, which are from here on referred to as IGA models.

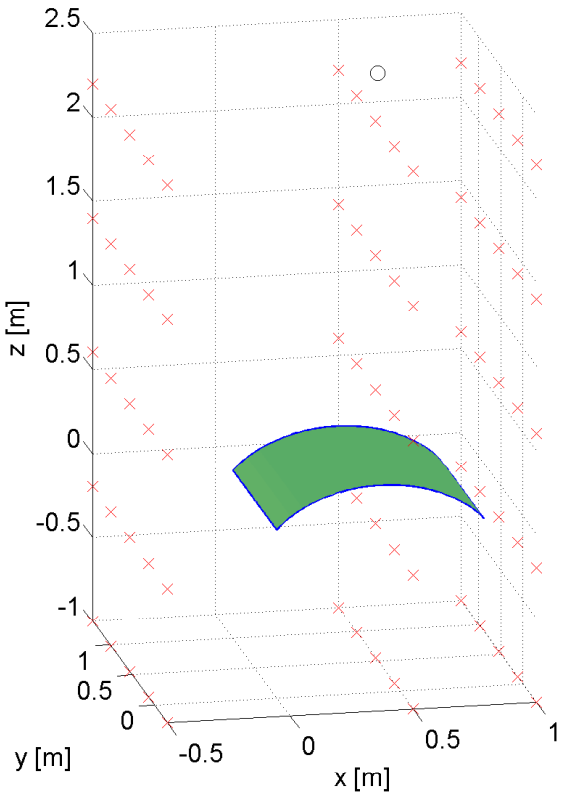

Coordinates:	x [m]	y [m]	z [m]
$\boldsymbol{r}_q$	0.5	0.5	2.5
$\boldsymbol{P}_1$	0	0	0
$\boldsymbol{P}_2$	0	1	0
$\boldsymbol{P}_3$	0.842	1	0
$\boldsymbol{P}_4$	0.842	0	0

Figure 3: The studied test case. ◯ indicates the acoustic point source location $\boldsymbol{r}_q$, × the response points. $\boldsymbol{P}_i$ $(i = 1, \ldots, 4)$ are the corner nodes of the curved panel.

They all use a quadratic NURBS basis, but have different numbers of elements, and therefore different amounts of degrees of freedom. The following IGA models are used:

- Model 1: quadratic NURBS mesh with 16 elements (as shown in Figure 5) resulting in 36 DOFs;
- Model 2: quadratic NURBS mesh with 144 elements, resulting in 196 DOFs;
- Model 3: quadratic NURBS mesh with 400 elements, resulting in 484 DOFs.

These models are compared to a conventional indirect variational Lagrangian BEM model which has a quadratic mesh of 144 elements, yielding 481 DOFs[2]. A very fine Lagrangian model is also created, which is used as a reference solution, with 2500 quadratic elements, yielding 7701 DOFs. The simulations of the IGA models are performed in MATLAB, while the Lagrangian calculations are done in LMS Sysnoise using `CQUAD8` elements. To compare the different models, the scattered pressure field is investigated. The average Frequency Response Function (FRF) over 75 response points (which are shown in Figure 3) is calculated from 50 to 500 Hz. This average FRF is given in Figure 4, showing coinciding curves, with a good overall match between all of them.

In order to better assess the performance of the different models, the relative error with respect to the reference model is investigated, according to the following formula:

$$\epsilon_{\text{avg}}\left(p_a\left(\boldsymbol{r}\right)\right) = \frac{1}{n_{\text{rp}}} \sum_{k=1}^{n_{\text{rp}}} \left| \frac{|p_a(\boldsymbol{r}_k)| - |p_{a,\text{ref}}(\boldsymbol{r}_k)|}{|p_{a,\text{ref}}(\boldsymbol{r}_k)|} \right|, \tag{23}$$

[2]This is a different amount of DOFs than the regular IGA model with the same number elements because both function bases are constructed differently. In general, for a given polynomial degree, a Lagrangian mesh will have more DOFs than a NURBS mesh with the same number of elements.

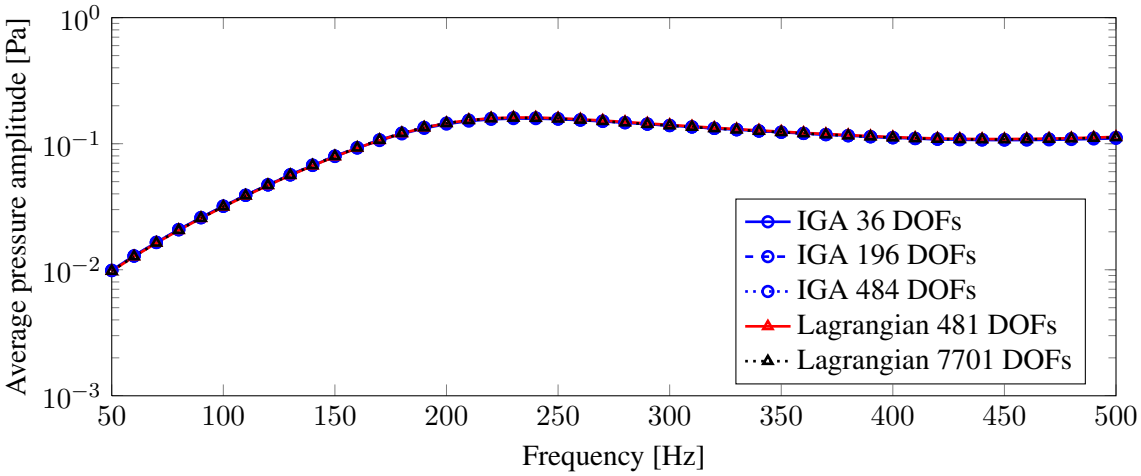

Figure 4: Average scattered field pressure amplitude over the 75 response points, with a frequency resolution of 10 Hz.

with $n_{\text{rp}} = 75$. Figure 6 shows the average error for the different models. These curves show that both the IGA models and the Lagrangian model are accurate, all satisfying engineering accuracy in the order of $1\,\%$. The IGA models mostly outperform the Langrangian ones (except for the very low frequency range, which is discussed below) with even the coarse IGA model with only 36 DOFs performing similarly to the Lagrangian model. Moreover, the two finer IGA models seem to have stopped converging, with their curves almost coinciding. These observations raise concern about the Lagrangian reference solution, which might not be accurate enough to properly assess the performance of the IGA models.

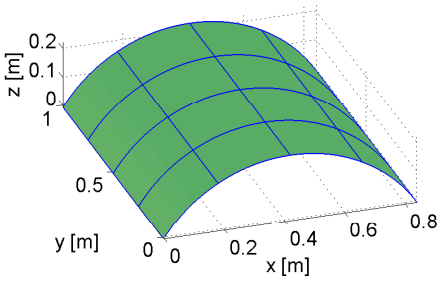

Figure 5: The NURBS mesh for the coarse IGA model. It consists of a quadratic NURBS patch with 16 elements, built up from 36 basis functions.

To further investigate this, the results are compared using the finest IGA model as a reference instead. This is shown in Figure 7, which also plots the error of the original Lagrangian reference model with 7701 DOFs. These curves indicate that the Lagrangian reference may indeed be the problem, as the IGA model 2 exhibits higher accuracy levels; the Lagrangian reference model poses the bottleneck in Figure 6. The curves in Figure 7 clearly indicate that the IGA models have a much higher accuracy per DOF than the Lagrangian model. Also in the higher frequency range, the proposed method still significantly outperforms the conventional Lagrangian BEM.

It should be noted that, although lower frequency results are generally expected to be more accurate than higher frequency ones, the IGA curves exhibit the opposite behaviour in Figure 6 in the lower frequency range. This can be explained by the low absolute values of the (reference) scattered pressure field for the lower frequencies — as Figure 4 shows. This drives the relative error upward, although the absolute error remains low. Indeed, plots of the absolute error values in Figures 8 and 9 confirm this, i.e. it is that low value of the reference pressure field used in equation (23) that leads to the higher relative error in this region.

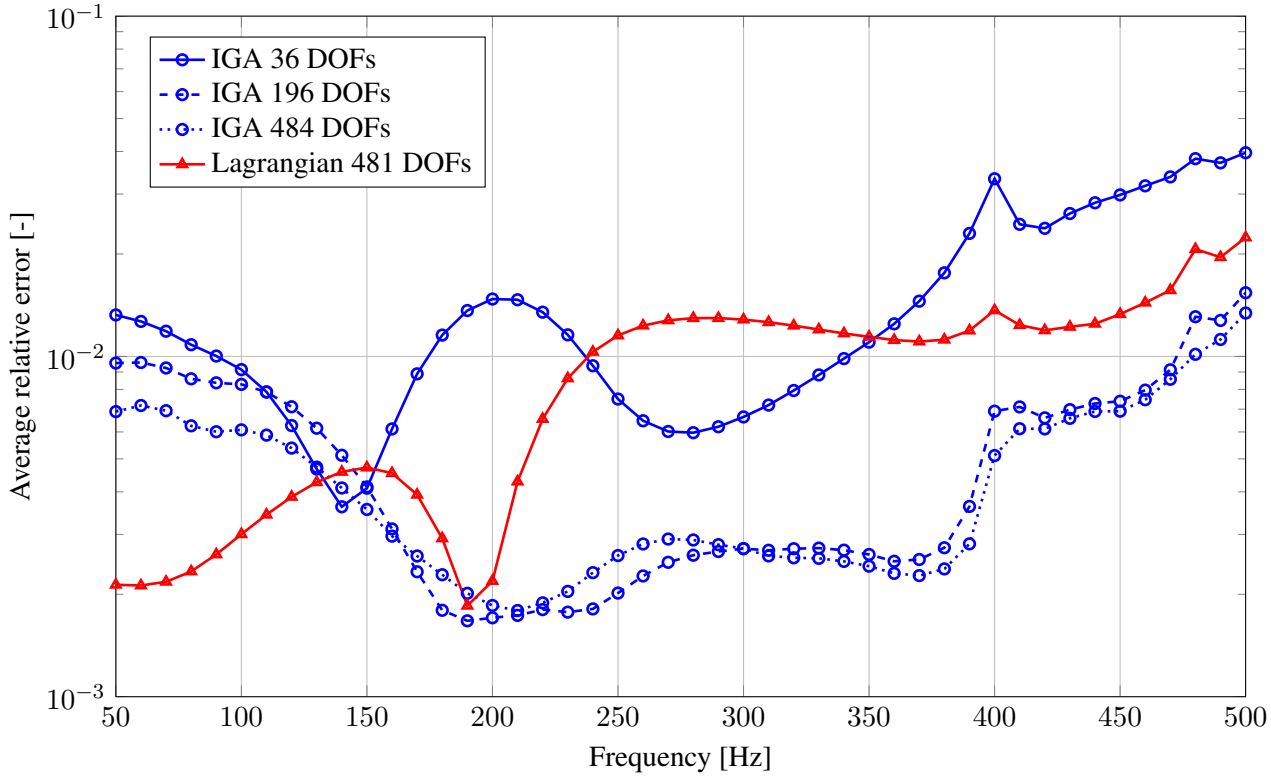

Figure 6: Relative error plot of the scattered pressure field for the different models with respect to a Lagrangian reference.

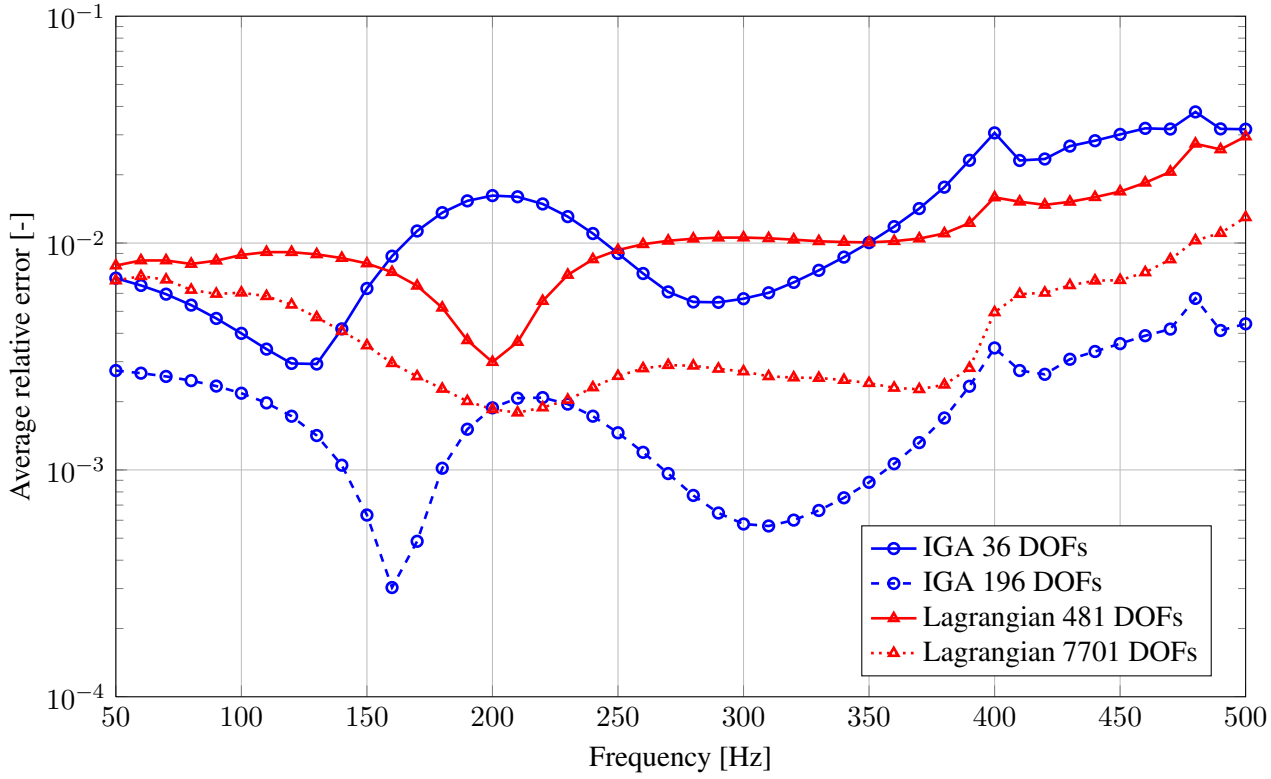

Figure 7: Relative error plot of the scattered pressure field for the different models with respect to an IGA reference.

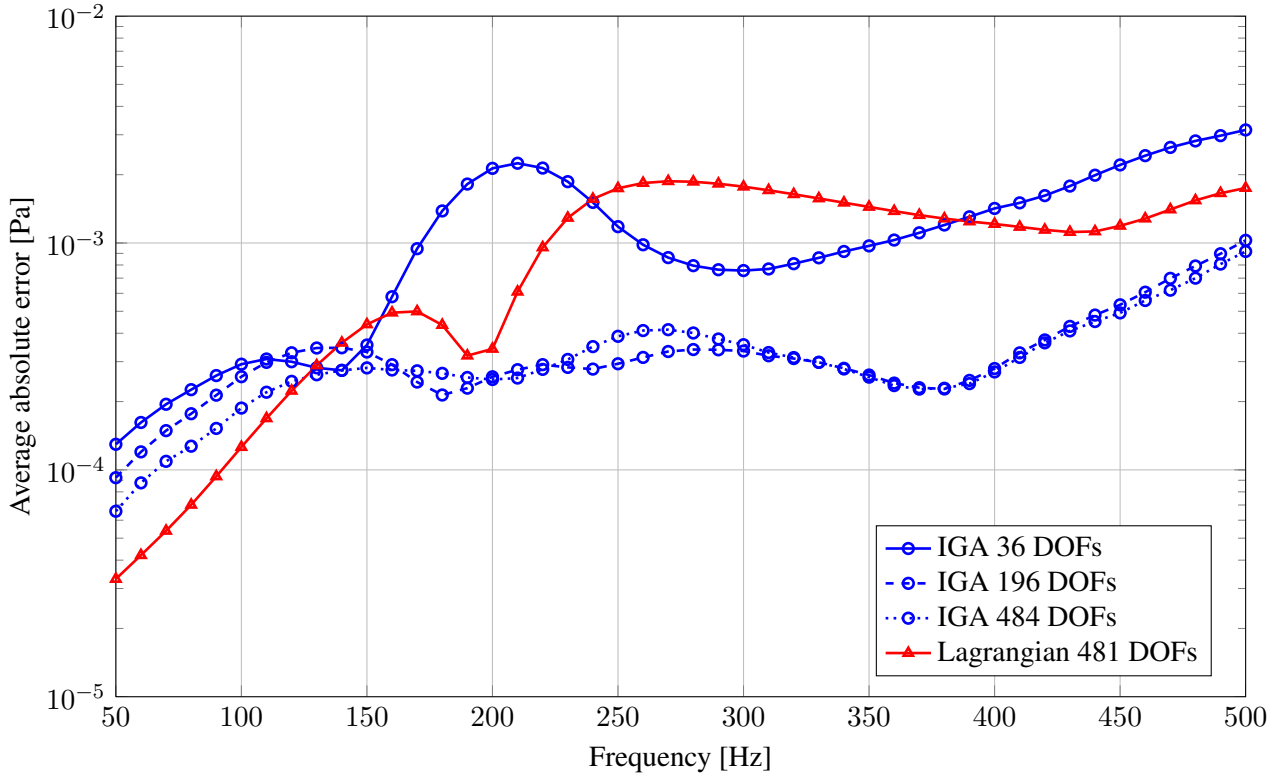

Figure 8: Absolute error plot of the scattered pressure field for the different models with respect to a Lagrangian reference.

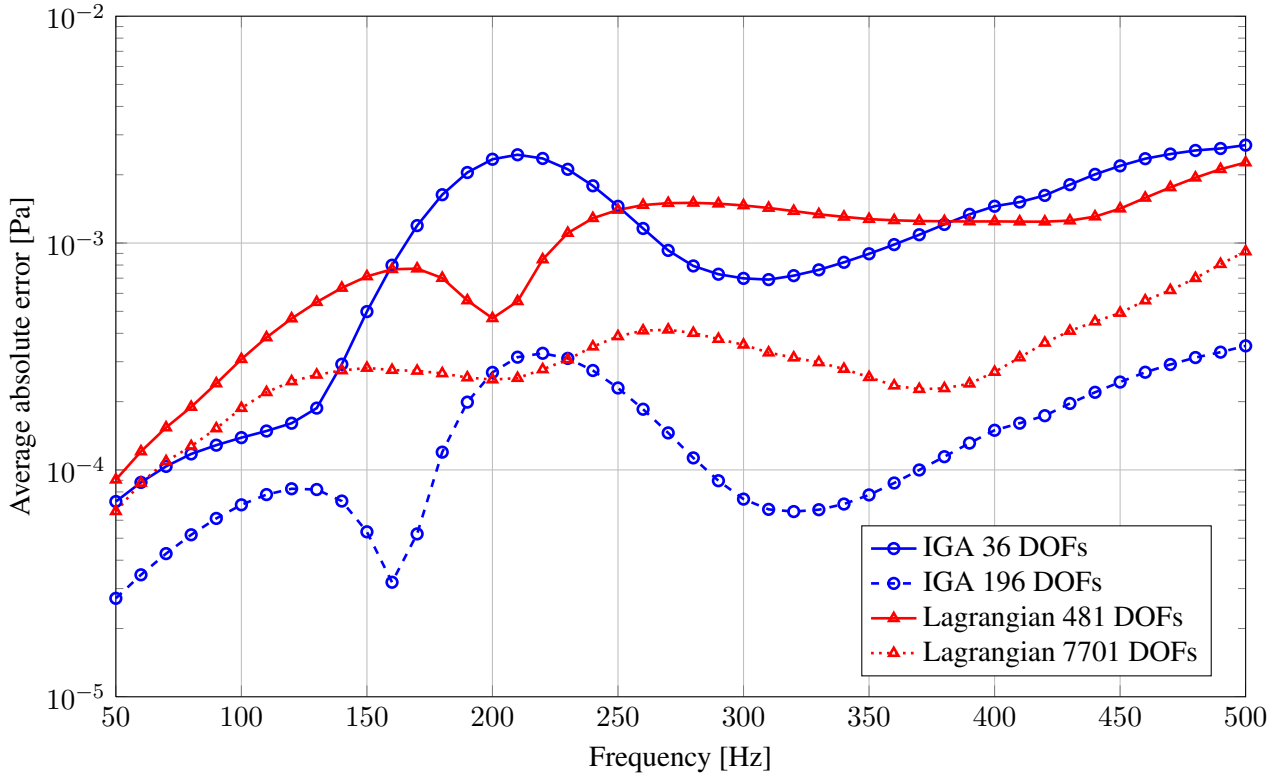

Figure 9: Absolute error plot of the scattered pressure field for the different models with respect to an IGA reference.

6 Conclusions

This paper presented an isogeometric indirect variational BEM for modelling steady-state acoustic problems. The new method was benchmarked against a conventional Lagrangian indirect variational BEM for a verification case with an open boundary surface, consisting of a rigid curved panel excited by a point source. The results showed that the proposed method compares very favorably, exhibiting a significantly higher accuracy per degree of freedom than the conventional Lagrangian BEM. The proposed method even outperformed a Lagrangian model with 40 times more DOFs.

Future work will further extend the benchmarks to higher frequencies. Also, the use of various polynomial orders will be examined, as well as problems with closed boundaries.

Acknowledgements

The research of Laurens Coox is funded by a PhD grant of the agency for Innovation through Science and Technology in Flanders (IWT-Vlaanderen). The authors also gratefully acknowledge IWT-Vlaanderen for their support of the ASTRA research project, and the KU Leuven Research Fund.

References

[1] O. Zienkiewicz, R. Taylor, *The Finite Element Method — The Three Volume Set*, Butterworth-Heinemann, 6th Ed. (2005).

[2] T. Wu, *Boundary Element Acoustics, Fundamentals and Computer Codes*, WIT Press (2000).

[3] T. Hughes, J. Cottrell, Y. Bazilevs, *Isogeometric analysis: CAD, finite elemens, NURBS, exact geometry and mesh refinement*, Computer Methods in Applied Mechanics and Engineering, Vol. 194, (2005), pp. 4135 – 4195.

[4] J. Cottrell, T. Hughes, Y. Bazilevs, *Isogeometric Analysis: Toward Integration of CAD and FEA*, John Wiley & Sons (2009).

[5] Y. Bazilevs, L. Beirão da Veiga, J. Cottrell, T. Hughes, G. Sangalli, *Isogeometric Analysis: approximation, stability and error estimates for h-refined meshes*, Mathematical Models and Methods in Applied Sciences, Vol. 16, (2006), pp. 1031 – 1090.

[6] J. Evans, Y. Bazilevs, I. Babuska, T. Hughes, *n-Widths, sup-infs, and optimality ratios for the k-version of the isogeometric finite element method*, Computer Methods in Applied Mechanics and Engineering, Vol. 198, (2009), pp. 1726 – 1741.

[7] J. Cottrell, A. Reali, Y. Bazilevs, T. Hughes, *Isogeometric analysis of structural vibrations*, Computer Methods in Applied Mechanics and Engineering, Vol. 195, (2006), pp. 5257 – 5296.

[8] J. Cottrell, T. Hughes, A. Reali, *Studies of refinement and continuity in isogeometric structural analysis*, Computer Methods in Applied Mechanics and Engineering, Vol. 196, (2007), pp. 4160 – 4183.

[9] F. Auricchio, L. Beirão da Veiga, A. Buffa, C. Lovadina, A. Reali, G. Sangalli, *A fully locking-free isogeometric approach for plane linear elasticity problems: A stream function formulation*, Computer Methods in Applied Mechanics and Engineering, Vol. 197, (2007), pp. 160 – 172.

[10] I. Akkerman, Y. Bazilevs, V. Calo, T. Hughes, S. Hulshoff, *The role of continuity in residual-based variational multiscale modelling of turbulence*, Computational Mechanics, Vol. 41, (2008), pp. 371 – 378.

[11] Y. Bazilevs, V. Calo, T. Hughes, A. Reali, G. Scovazzi, *Variational multiscale residual-based turbulence modeling for large eddy simulation of incompressible flows*, Computer Methods in Applied Mechanics and Engineering, Vol. 197, (2007), pp. 173 – 201.

[12] Y. Zhang, Y. Bazilevs, S. Goswami, C. Bajaj, T. Hughes, *Patient-specific vascular NURBS modeling for isogeometric analysis of blood flow*, Computer Methods in Applied Mechanics and Engineering, Vol. 196, (2007), pp. 2943 – 2959.

[13] R. Simpson, M. Scott, M. Taus, D. Thomas, H. Lian, *Acoustic isogeometric boundary element analysis*, Computer Methods in Applied Mechanics and Engineering, Vol. 269, (2014), pp. 265 – 290.

[14] M. Scott, R. Simpson, J. Evans, S. Bordas, T. Hughes, T. Sederberg, *Isogeometric Boundary element analysis using unstructured T-splines*, Computer Methods in Applied Mechanics and Engineering, Vol. 254, (2013), pp. 197 – 221.

[15] R. Simpson, S. Bordas, H. Lian, J. Trevelyan, *An isogeometric boundary element method for elastostatic analysis: 2D implementation aspects*, Computers and Structures, Vol. 118, (2013), pp. 2 – 12.

[16] P. Morse, K. Ingard, *Theoretical Acoustics*, Princeton University Press (1968).

[17] L. Piegl, W. Tiller, *The NURBS Book*, Springer-Verlag Berlin Heidelberg (1997).